

# UNCLASSIFIED

AD NUMBER
ADB232924
NEW LIMITATION CHANGE
TO Approved for public release, distribution unlimited
FROM Distribution authorized to U.S. Gov't. agencies only; Proprietary Information; Oct 97. Other requests shall be referred to US Army Medical Research and Materiel Command, 504 Scott St., Fort Detrick, MD 21702-5012.
AUTHORITY
USAMRMC ltr, 23 Aug 2001

THIS PAGE IS UNCLASSIFIED

AD \_\_\_\_\_

GRANT NUMBER DAMD17-96-1-6283

TITLE: High Fidelity Electronic Display of Digital Mammographs

PRINCIPAL INVESTIGATOR: Michael J. Flynn, Ph.D.

CONTRACTING ORGANIZATION: Henry Ford Health Systems  
Detroit, Michigan 48202-2689

REPORT DATE: October 1997

TYPE OF REPORT: Annual

PREPARED FOR: Commander  
U.S. Army Medical Research and Materiel Command  
Fort Detrick, Maryland 21702-5012

DISTRIBUTION STATEMENT: Distribution authorized to U.S. Government agencies only (proprietary information, Oct 97). Other requests for this document shall be referred to U.S. Army Medical Research and Materiel Command, 504 Scott Street, Fort Detrick, Maryland 21702-5012.

The views, opinions and/or findings contained in this report are those of the author(s) and should not be construed as an official Department of the Army position, policy or decision unless so designated by other documentation.

19980130 151

# REPORT DOCUMENTATION PAGE

Form Approved  
OMB No. 0704-0188

Public reporting burden for this collection of information is estimated to average 1 hour per response, including the time for reviewing instructions, searching existing data sources, gathering and maintaining the data needed, and completing and reviewing the collection of information. Send comments regarding this burden estimate or any other aspect of this collection of information, including suggestions for reducing this burden, to Washington Headquarters Services, Directorate for Information Operations and Reports, 1215 Jefferson Davis Highway, Suite 1204, Arlington, VA 22202-4302, and to the Office of Management and Budget, Paperwork Reduction Project (0704-0188), Washington, DC 20503.

1. AGENCY USE ONLY (Leave blank)		2. REPORT DATE October 1997	3. REPORT TYPE AND DATES COVERED Annual (3 Sep 96 - 2 Sep 97)	
4. TITLE AND SUBTITLE High Fidelity Electronic Display of Digital Mammographs			5. FUNDING NUMBERS DAMD17-96-1-6283	
6. AUTHOR(S) Michael J. Flynn, Ph.D.				
7. PERFORMING ORGANIZATION NAME(S) AND ADDRESS(ES) Henry Ford Health Systems Detroit, MI 48202-2689			8. PERFORMING ORGANIZATION REPORT NUMBER	
9. SPONSORING/MONITORING AGENCY NAME(S) AND ADDRESS(ES) Commander U.S. Army Medical Research and Materiel Command Fort Detrick, Frederick, Maryland 21702-5012			10. SPONSORING/MONITORING AGENCY REPORT NUMBER	
11. SUPPLEMENTARY NOTES				
12a. DISTRIBUTION / AVAILABILITY STATEMENT DISTRIBUTION STATEMENT: Distribution authorized to U.S. Government agencies only (proprietary information, Oct 97). Other requests for this document shall be referred to U.S. Army Medical Research and Materiel Command, 504 Scott Street, Fort Detrick, Maryland 21702-5012.			12b. DISTRIBUTION CODE	
13. ABSTRACT (Maximum 200)  We are investigating photoemissive structures which can achieve the required display performance of digital mammography. A thin glass faceplate supported by a glass microcapillary array is being studied. The objectives of this project we are modeling the performance , constructing a test fixture, designing an emissive structure, and obtaining preliminary experimental data. With respect to performance modeling we have; 1) developed software to describe the electric field and the trajectories of electrons and used it to study the effect of the focusing plate electrode, 2) used electron/photon transport computations to characterize the electron backscattering from phosphor layers, and 3) developed a simulation code to study the luminance spread function of emissive structures and reported results for conventional CRT structures and for thin structures. With respect to the test system we have; 1) designed and constructed the vacuum subsystem and experimental chamber into which will be mounted a cathode and emissive structure, and 2) designed a cone shaped luminance probe that will measure spread function tails on actual emissive structures. During the first year of the project we have completed the planned simulation work and the construction of a test system is on schedule.				
14. SUBJECT TERMS Breast Cancer Mammography      Display			15. NUMBER OF PAGES 30	
DTIC QUALITY INSPECTED 2			16. PRICE CODE	
17. SECURITY CLASSIFICATION OF REPORT Unclassified	18. SECURITY CLASSIFICATION OF THIS PAGE Unclassified	19. SECURITY CLASSIFICATION OF ABSTRACT Unclassified	20. LIMITATION OF ABSTRACT Limited	

## FOREWORD

Opinions, interpretations, conclusions and recommendations are those of the author and are not necessarily endorsed by the U.S. Army.

✓ Where copyrighted material is quoted, permission has been obtained to use such material.

✓ Where material from documents designated for limited distribution is quoted, permission has been obtained to use the material.

✓ Citations of commercial organizations and trade names in this report do not constitute an official Department of Army endorsement or approval of the products or services of these organizations.


\_\_\_\_ In conducting research using animals, the investigator(s) adhered to the "Guide for the Care and Use of Laboratory Animals," prepared by the Committee on Care and Use of Laboratory Animals of the Institute of Laboratory Resources, National Research Council (NIH Publication No. 86-23, Revised 1985).

\_\_\_\_ For the protection of human subjects, the investigator(s) adhered to policies of applicable Federal Law 45 CFR 46.

\_\_\_\_ In conducting research utilizing recombinant DNA technology, the investigator(s) adhered to current guidelines promulgated by the National Institutes of Health.

\_\_\_\_ In the conduct of research utilizing recombinant DNA, the investigator(s) adhered to the NIH Guidelines for Research Involving Recombinant DNA Molecules.

\_\_\_\_ In the conduct of research involving hazardous organisms, the investigator(s) adhered to the CDC-NIH Guide for Biosafety in Microbiological and Biomedical Laboratories.

  
PI - Signature

  
Date

DAMD17-96-1-6283  
Progress Report - Year 1

High Fidelity Electronic Display of Digital Mammograms  
PI: Michael J. Flynn, PhD.

Pg i. Front Cover

Pg ii Form 298

Pg iii. Foreword

Pg iv. Table of Contents

Pg 1. Introduction

Pg 3. Body: Year One Progress Report

Pg 10. Conclusions

Pg 11. References

Appendix A: Vacuum subsystem (plus 1 pgs)

Appendix B: SPIE 1997 Publication (plus 10 pgs)

Appendix C: SID 1997 Publication (plus 4 pgs)

# 1 INTRODUCTION

This project involves the development of methods for "High Fidelity Electronic Display of Digital Mammographs". Cathodoluminescent medical image displays are considered including specialized cathode ray tubes and flat panel displays using cold cathode emitters and microvacuum cells (fig. 1). For field emitter display devices, a small cathode generates a regulated pulse of electrons which is accelerated across a vacuum gap to a photoemissive layer. We are focusing in this project on the visual performance of the photoemissive layer.

The objective of our research is to establish that advanced designs for the emissive structure of cathodoluminescent display devices can achieve the performance required for viewing computer images obtained from digital mammography systems. The approach being investigated is to building the photoemissive Conventional CRT devices are not capable of meeting the stringent display requirements of medical mammography because of the thick glass in the emissive structure. We think that a microchannel photoemissive assembly can achieve the needed display performance. We are now optimizing the design of the photoemissive assembly. We will next experimentally establishing the ability to achieve high brightness, high resolution and low glare with a wide dynamic range.

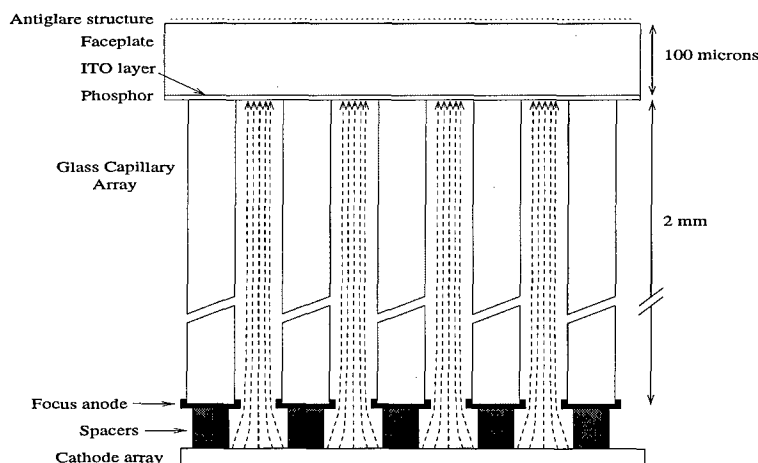


Figure 1: Photoemissive emissive structure model.

In most display devices, image degradation can be traced to processes associated with the transport of light from the point of generation and to the optical properties of the emission surface. Transilluminated film, one of the highest fidelity display devices available, modulates the light intensity by diffusion in the layer of dense silver grains in the emulsion. This layer is at the outer surface and separated only by a thin overcoat from the surface. Consequently, there is

little lateral transport of light which would degrade contrast or resolution. Additionally, the overcoat has a rough surface causing diffuse scatter of ambient light and minimal surface glare.

We seek a photoemissive assembly which generates light very near the surface and with a rough outer surface so as to appreciate the same high fidelity as obtained with transilluminated film. The general approach we are using involves the use of a glass microchannel plate with an overall thickness of 2 to 3 mm. As illustrated in fig. 1, electrons from the cathode elements are directed into the microchannels to a thin phosphor layer deposited on glass with a thickness of about 100 microns, i.e. similar to that of the cover plates used in conventional microscope slides. Structural rigidity is provided by the microchannel plate.

## 2 Body: Year One Progress

This project involves four technical objectives:

- Model the photoemissive performance of microchannel assemblies.
- Fabricate a test system.
- Design and construct a microchannel emissive structure.
- Perform experimental tests and compare with model calculations.

The first two objectives have been pursued during the first year of the project as was planned in the application. Our progress in these two areas is summarized in the following.

### 2.1 Photoemissive performance modeling

The first technical objective was the performance modeling of the proposed emissive structure assembly. The simulation of device performance relates to 3 different aspects which differ both in the physical processes as well as in the applied methods:

- Predicting electron trajectories in the vacuum cell,
- Predicting electron energy deposition in the emissive layers, and
- Simulation of the light transport processes in the emissive structure.

For each aspect of performance modeling we describe in the following, the advancements and developments and results made during this first half of the project that contributed to obtaining significant insight on the performance of the proposed emissive structure design.

#### 2.1.1 Modeling electron trajectories in vacuum cells

##### Methods

To study the effect of the capillary array on the electron trajectories in the proposed design, we have developed a simulation code (ELECTRA) that computes the solution to the Poisson's equation using a finite-difference approach and an over-relaxation technique. For the analysis of the impact of the capillary structure, the full 3D solution may be obtained using a cylindrical coordinate system, by aligning the axis of symmetry with the axis of the capillary tube, when appropriate boundary conditions are used.

An important aspect of computing potential solutions in vacuum cells for the simulation of electron trajectories is the use of an appropriate mesh size. Large



array sizes provide accuracy while increasing the computing time in a non-linear fashion with respect to array dimensions. To achieve good solutions for the electric potential, we implemented a 3-stage computation scheme (low-resolution, medium-resolution, and high-resolution). By computing the solution at each step, and using a bicubic spline technique to interpolate the expanded solution, we were able to significantly reduced the computing time for a given solution, and obtain convergence much faster.

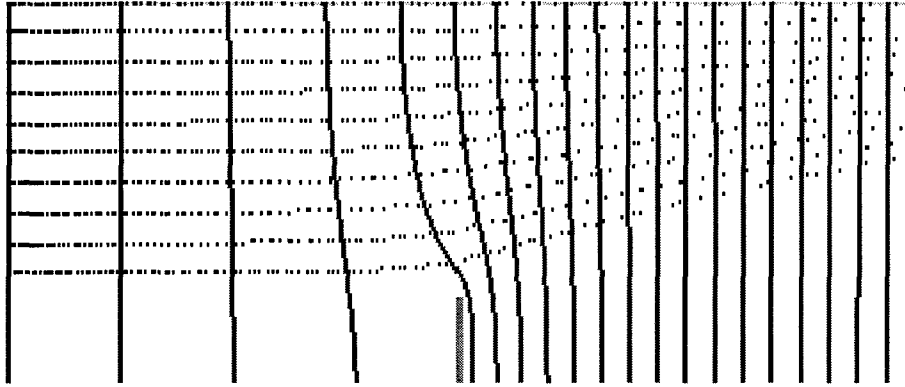


Figure 2: Isocontour plot for a region close to the focusing plate.

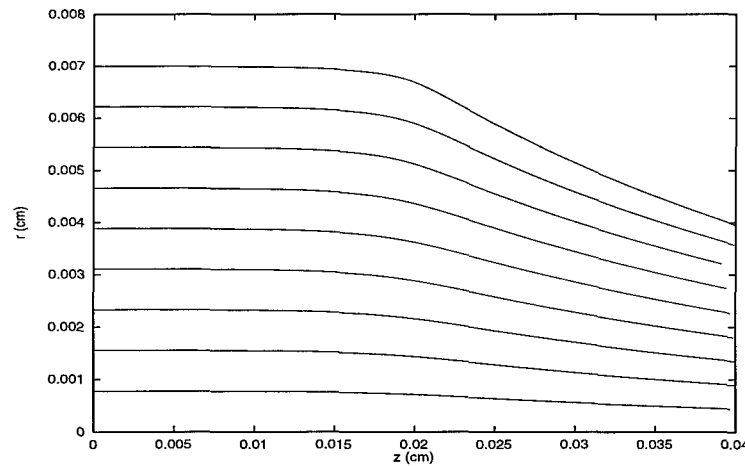


Figure 3: Electron trajectories generated with ELECTRA for a region close to the focusing plate.

To determine when the iteration has converged to an acceptable solution, the residual at a given point in the solution array is reported. Typical values of

$10^{-3}$  have shown to be acceptable criteria for the studied cases.

The program generates electron trajectories using the Burlish-Stoer method to solve the equation of motion with adaptable time steps.[9] The results are presented in isocontour plots and trajectory data files (fig. 2 and 3).

### Results

We have applied ELECTRA to study the effect of the focusing plate electrode for the proposed design. For a 3 mm thick structure, a 1 mm thick microcapillary array with a 1 kV total acceleration voltage and focusing metal electrode at  $V_f$  was considered. The metal electrode enters the channel up to a diameter length, i.e. 50  $\mu\text{m}$ . Electrons are assumed to be emitted from the cathode forming a parallel extended beam for normal incidence into the microcapillary array. This can be achieved with an emitting surface such as a field emitter cathode structure, or with a point emitter and appropriate electron optics components. The goal is to adjust  $V_f$  in order to alter the trajectories to direct the electrons into the tubes, while minimizing the impacts on the focusing electrode plate and on lateral tube walls (see next section for a discussion on secondary electron emission).

### Problems encountered

A potential problem with the approach being used involves the charging of insulators in vacuum under electron bombardment which has been studied by several authors. [7, 6, 1] When an energetic electron hits an insulator, multiple secondary electrons are generated. A fraction of them are directed back into the vacuum. This fraction is called "true" secondary electron emission. Energetic backscattered electrons can travel significant distances away from the initial landing site. The low-energy electrons however, can in some scenarios, be directed back against the surface, creating charge accumulation in the superficial layers of the insulator material. This surface charge density may in turn affect the local electric fields, up to a point where a self-sustaining equilibrium is achieved. In this case, a secondary electron emission of 1 is required. When electric fields are parallel to the insulator surface, a net current can be observed which is explained by a hopping transport mechanism.[8]

Inside capillaries, the electric field is normally oriented parallel to the insulator surface. Two different cases can be studied. In the first, an energetic electron may hit directly the interior wall of the tube, before reaching the phosphor layer. Such an event will generate multiple less energetic secondary electrons that will eventually reach the anode. This condition is not favorable to an efficient electron energy to luminescence conversion, and thus its occurrence has to be minimized by using an appropriate voltage  $V_f$ . The second case relates to the backscattered electrons coming from the phosphor material that may hit the surfaces of the tube. In this case, the wide range of electron energies and angles of interaction will determine the ability of the system to reach the equilibrium point.

Similar scenarios are encountered in other technologies related to emissive displays. For instance, Micron Display Technologies, Inc. has recently reported the use of high aspect ratio glass posts for spacing the cathode structure from the anode layers. [4] The use of a thin resistive layer coated onto the inner walls of the tubes may constitute a solution to this problem, although a mechanism for controlling the resistivity of a thin layer, as well as a suitable coating technique have not been disclosed.

This problem was not recognized at the beginning of this project. At the present time, we are addressing the issue of surface charging by using simulation methods to describe the energy and angular distribution of secondary electrons. We will also determine experimentally under what circumstances an energetic beam will travel through the tube without losses.

### **2.1.2 Electron energy deposition modeling**

#### **Glare from backscattered electrons**

Our laboratory previously developed an electron/photon transport code, SKEPTIC [5, 10], specifically intended to model low energy electron transport. We have used SKEPTIC to characterize the electron backscattering from the phosphor layer of an emissive structure. In CRT devices, the backscattered component that returns into the vacuum, may hit the phosphor layer at significant distances from the original landing site, and generate a diffuse signal. We have completed computations to document the effect of this backscattering on image glare. For this, we used actual layer material specifications including the aluminum conductive film on top of the phosphor grains, and the conductive coatings on the inside of the tube. We have used a typical broad band ZnO:Zn phosphor for the simulations. Preliminary results show that the tails of the line-spread function for incidence at the center will not affect significantly the image quality of the displayed data (fig. 4). However, in color CRTs, grille apertures or shadow masks may interfere the backscattered electrons and generate a more important and local degradation effect.

#### **Electrons backscattered in channels**

We are now using SKEPTIC to model the angular and energy distribution of backscattered electrons coming from the interaction of energetic electrons with the phosphor in the proposed emissive structure design. This will contribute to the description of the physics of electrons traveling inside the microcapillary array, and the effect of backscattering on surface charging.

## **2.2 Modeling of light transport in emissive structures**

We have developed a Monte Carlo simulation code (DETECT-II) to study the luminance spread functions of emissive structures. The unique features of the

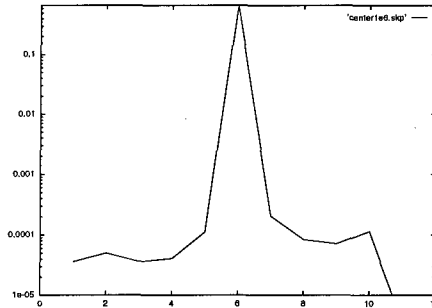


Figure 4: Line-spread function of backscattered electron diffuse signal for a typical monochrome CRT.

code, as well as the results for typical CRT and flat emissive display structures have been reported. [2, 3].

In addition, simulation of degradation of image quality by glare using 2D Fast Fourier Transform over large image arrays ( $2048 \times 2048$ ) was performed. The application of this method to digital radiographs was described recently. [2] We refer to the proceeding papers which are attached as appendices for a complete description of these methods and results.

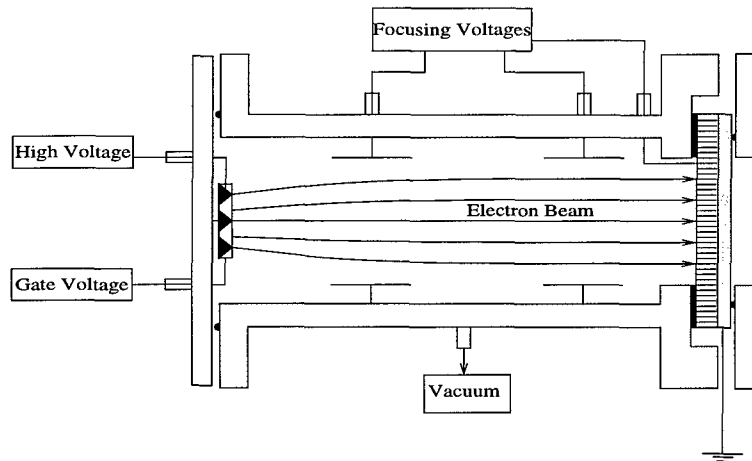


Figure 5: Test device assembly for testing photoemissive emissive structure.

### 2.2.1 Model validation

We have reported the glare for both thick and thin emissive structures in the papers noted above. We are now performing experiments on sections of thick

structures extracted from medical imaging CRT devices. These experiments will establish the accuracy of our models as well as document the performance deficit of current CRT devices.

## 2.3 Fabrication of a test system

### 2.3.1 Vacuum subsystem

The test system for emissive structures being built consists of a vacuum chamber with a cathode at one end and an emissive structure installed at the other end. Tests are planned in which a pattern will be placed on the back surface of the emissive structure to enable resolution and glare to be measured. Used in the manner, the cathode needs only to produce a uniform beam of electrons with no dynamic pattern.

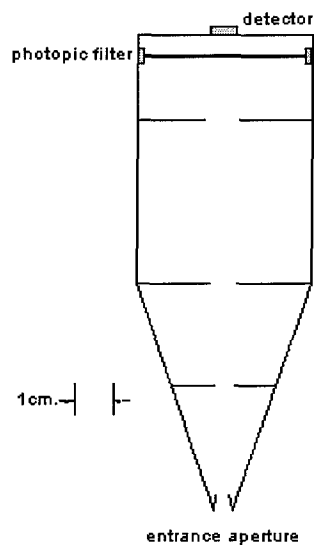


Figure 6: Cone-shaped probe for glare measurements.

The design of the vacuum system has been completed all components are now being installed in our laboratory. This includes a low vacuum mechanical pump, a high vacuum turbopump, high and low vacuum gauges, and an experimental chamber. The configuration of the vacuum subsystem is detailed in an attached appendix.

### 2.3.2 Glare performance measurements

Measurements of glare, particularly for systems with low glare, require measurement systems which do not contribute to the observed glare. The measurements

we proposed were to all be done with a CCD observation system. This will still be used for measurements of resolution and noise. For glare measurements we have designed an optical probe to be used with a laboratory photometer. The cone shaped luminance probe will be used to measure luminance spread function tails of actual emissive structures both in the test system and conventional display devices (fig. 6).

### 3 CONCLUSIONS

During the first half of the project we have advanced the simulation tools to characterize electron and optical transport in emissive structures. By using the simulation tools, we have advanced our understanding of the degrading effects of the luminance spread in thick emissive structures.

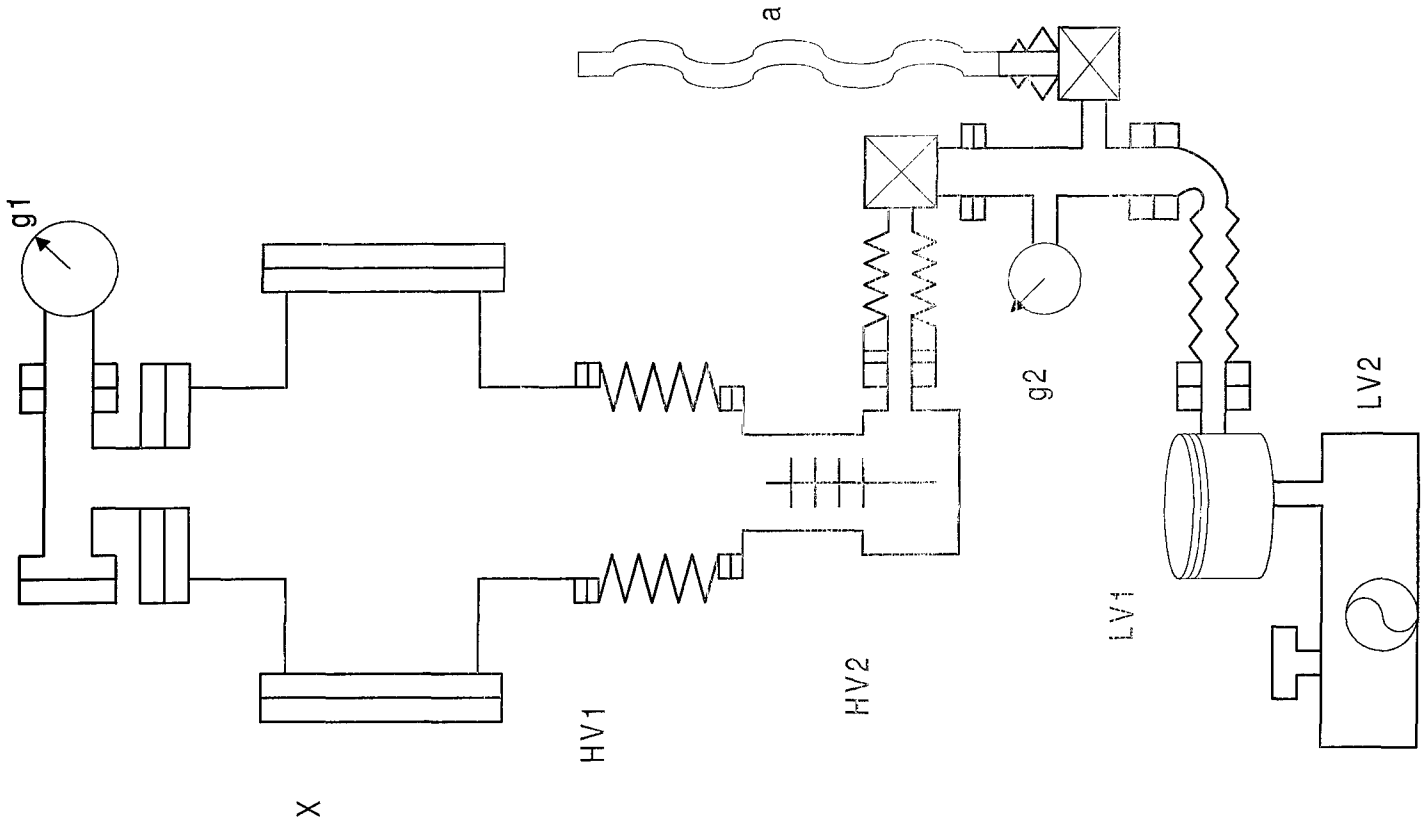
In the next half, we will demonstrate our findings on improved display performance of such an emissive structure by measuring the characteristics of a test device (fig. 5) that will consist of a parallel extended electron beam and the proposed emissive structure with the microcapillary array backing the anode phosphor layer.

## References

- [1] C. Attard and J. P. Ganachaud. Study of the space charge induced by an electron beam in an insulating target ii. presentation of the results. *Physica Status Solidi*, 199:455–465, 1997.
- [2] A. Badano and M. J. Flynn. Image degradation by glare in radiologic display devices. In *SPIE Medical Imaging 1997: Image Display*, 1997. .
- [3] A. Badano and M. J. Flynn. Monte carlo modeling of the luminance spread function in flat panel displays. In *IDRC 1997*, pages 382–385, 1997. .
- [4] J. Browning, C. Watkins, J. Alwan, and J. Hoffman. Scaling of FED technology. In *IDRC 1997*, pages F-42, 1997. .
- [5] M. J. Flynn, S. M. Hames, S. J. Wilderman, and J. J. Ciarelli. Quantum noise in digital X-ray imaging detectors with optically coupled scintillators. *IEEE Transactions on Nuclear Science*, 1996. accepted for publication 2-19-96.
- [6] J. P. Ganachaud, C. Attard, and R. Renoud. Study of the space charge induced by an electron beam in an insulating target i. monte carlo simulation method. *Physica Status Solidi*, 199:175–184, 1997.
- [7] J. P. Ganachaud and A. Mokrani. Theoretical study of the secondary electron emission of insulating targets. *Surface Science*, 334:329–341, 1995.
- [8] B. H. W. Hendriks, G. G. P. van Gorkom, N. Lambert, and S. T. de Zwart. Modes in electron-hopping transport over insulators sustained by secondary electron emission. *Journal of Physics D: Applied Physics*, 30:1252–1264, 1997.
- [9] W. H. Press, S. A. Teukolsky, W. T. Vetterling, and B. P. Flannery. *Numerical recipes in C*. Cambridge University Press, 1992.
- [10] S. J. Wilderman, S. M. Hames, M. J. Flynn, and W. R. Martin. Monte Carlo calculation of X-ray spectra emitted by various anode materials at low voltages. In *IEEE Nuclear Science Symposium NSS'94*, 1994.



# Appendix A



X: Experimental Chamber  
g1: Active Inverted Magnetron Gauge  
g2: Active Pirani Gauge  
HV1: Vibration Isolator  
HV2: Turbo Pump  
LV1: Foreline Trap  
LV2: Roughing Pump  
a: accessory line and vent

XIRL - - P00.97.00

Title: Vacuum Subsystem  
Date: 10/01/97  
Rev: 00 By: Y.Yu

Henry Ford Health System

## Appendix B

# Image Degradation by Glare in Radiologic Display Devices

Aldo Badano and Michael J. Flynn

X-Ray Imaging Research Laboratory  
Henry Ford Health System, Detroit, Michigan

Department of Nuclear Engineering and Radiological Sciences  
University of Michigan, Ann Arbor, Michigan

## ABSTRACT

No electronic devices are currently available that can display digital radiographs without loss of visual information compared to traditional transilluminated film. Light scattering within the glass faceplate of cathode-ray tube (CRT) devices causes excessive glare that reduces image contrast. This glare, along with ambient light reflection, has been recognized as a significant limitation for radiologic applications. Efforts to control the effect of glare and ambient light reflection in CRTs include the use of absorptive glass and thin film coatings. In the near future, flat panel displays (FPD) with thin emissive structures should provide very low glare, high performance devices. We have used an optical Monte Carlo simulation to evaluate the effect of glare on image quality for typical CRT and flat panel display devices. The trade-off between display brightness and image contrast is described. For CRT systems, achieving good glare ratio requires a reduction of brightness to 30-40 % of the maximum potential brightness. For FPD systems, similar glare performance can be achieved while maintaining 80 % of the maximum potential brightness.

**Keyword List:** flat panel display, emissive display, digital radiography, CRT, glare.

## 1 INTRODUCTION

The radiologic information acquired by current digital radiographic systems is often interpreted using film from a laser printer. The electronic display of digital radiographs will require devices with the performance of transilluminated film.<sup>1</sup> High luminance, low noise and wide dynamic range are required, as summarized in Table I. Computer workstations designed for displaying and interpreting digital radiographs all use cathode-ray tube monitors (CRT). However, the limitations of current CRT display devices as compared to transilluminated film have been recognized and include issues such as brightness, resolution, dynamic range, uniformity, and noise.<sup>2-6</sup>

Typical CRTs require a thick glass panel between the light emission sites and the viewer. Depending on the curvature ratio of the tube, the faceplate thickness may range between 1.3 and 2.5 cm.<sup>7</sup> Multipath light scattering in the faceplate adds a diffuse background (glare) to the primary signal that reduces contrast. The degradation

Total dimensions	35 cm x 43 cm
Pixel dimensions	160 $\mu\text{m}$ max. / 80 $\mu\text{m}$ nominal
Array size	2000 x 2500 min. / 4000 x 5000 nominal
Peak luminance	2000 $\text{cd}/\text{m}^2$
Minimum luminance	5 $\text{cd}/\text{m}^2$
Color	white
Emission distribution	lambertian
Noise power spectrum	white
S/N for each pixel	> 100
S/N for .5 mm region	> 400
Intrascene dynamic range	400
Greyscale	1024 (log or perceptually linear)
Refresh rate	static or 70 Hz
Large area distortion	1 %
Color inversion	none

Table 1: High fidelity display requirements

in image quality is significantly more severe for subtle lesions in dark regions with bright surroundings. To reduce the contrast reduction by glare, dark tinted glass is used for the faceplate. Transmission can be as low as 13 % for a thickness of 1.78 cm (equivalent to an absorption coefficient of  $1.15 \text{ cm}^{-1}$ ).<sup>8</sup> On the other hand, flat panel field-emission displays<sup>9-13</sup> have the potential for a thin faceplate due to a large number of spacers between the electron emitting layer and the phosphor. In this paper, the low frequency degradation of image quality by glare from light scattering in the faceplate of emissive display devices is addressed. The effect of glare for both CRT and flat panel display emissive structures is computationally modeled for test pattern images. Finally, the influence of glare-reducing glass absorbers on both glare and display brightness is reported.

## 2 GLARE IN EMISSIVE DISPLAYS

Computational models have been used to simulate the effect of device characteristics on display performance including the frequency response of electronics, electron beam spot size, and phosphor granularity.<sup>14,15</sup> Computational modeling can also be used to simulate glare. This requires accurate knowledge of all processes that propagate light from bright spots in an image to points at substantial distance, i.e. the tails of the device point spread function (PSF). This work has been motivated by a desire to obtain accurate PSFs to model glare. While the tails of these PSFs can have very low values, they can contribute significant signal because of their spatial extent.

Glare measurements on actual CRT emissive structures have been recently reported.<sup>16</sup> These glare measurements and glare measurement results are strongly dependent on the nature of the test image. However, no standard metric has been adopted for reporting the glare characteristics of actual display devices. In this study, a test pattern that we previously described was used.<sup>17</sup> The pattern consists of an inner dark circular spot, surrounded by a bright outer circle with a ratio of radii of 10. The rest of the scene is kept at the same dark level of the inner spot (see Fig. 1). The glare ratio is defined as the difference in display luminance between the central pixel in the pattern and the brightest pixel in the bright region.

The impact of electron backscattering on display performance has not been considered in previous studies. For an Al layer, the backscattering fraction for an electron beam energy of 10 keV is about 12.5-15 % and 14-15 % for 30 keV.<sup>18,19</sup> The backscattered electrons are subjected to the electromagnetic fields present in the

vacuum region. The backscattered electrons will eventually impinge on the phosphor at a distance from its initial interaction position which is a function of the backscattering angle and energy. The backscattering energy, which is a function of the backscattering angle, will eventually result in the backscattered electron impinging into the phosphor at a certain distance from its initial interaction position. This results in an electronic contribution to glare that is not considered in this work.

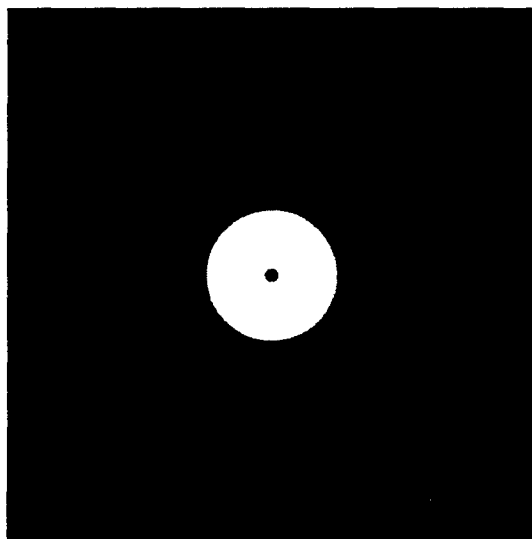


Figure 1: Test pattern for glare measurements.

### 3 MODELING GLARE IN DISPLAY DEVICES

#### 3.1 Monte Carlo calculation of the point spread function

In a cathodoluminescent display device, the emissive structure includes all components that convert energetic electrons to visible light. Typical emissive structures components include: cathodoluminescent phosphors, conductive layers, reflective or absorptive films, transparent support (faceplate), and anti-reflective and anti-glare materials. In this work, we have modeled the glare characteristics of 2 types of emissive structures. All surfaces are modeled as perfectly flat. The angular distribution emerging from the phosphor layer was assumed to be lambertian.

Structures CRT-A and CRT-B are typical CRT display devices. Both have a faceplate thickness of 1.6 cm. CRT-A has an Al conductive and reflective layer on the back of the phosphor layer producing a reflection of 90 %. CRT-B has a perfectly absorbing black matrix coated in between the phosphor dots, with an aperture ratio of 50 %. For each CRT structure, 5 levels of absorption coefficient were considered (0.0, 0.2, 0.4, 0.6, and  $1.0 \text{ cm}^{-1}$ ). Emissive structures FPD-A and FPD-B are typical of flat-panel emissive displays. The thicknesses are 0.3 and 0.1 cm respectively. For each FPD structure, 8 levels of absorption coefficient were considered (0.0, 0.2, 0.4, 0.6, 1.0, 3.0, 5.0 and  $9.0 \text{ cm}^{-1}$ ). Cross-sections of the emissive structures are presented in figures 2 and 3.

In previous work, we described Detect-II, an optical Monte Carlo code, capable of simulating the optical transport processes in emissive structures. Unique features of the code include special binning for simulating display performance characteristics, and photon polarization tracking.<sup>17</sup> Detect-II was used to obtain the PSFs of different emissive structures. The results of the Monte Carlo calculation yield the number of photons,  $P_0$ , that originate from the source point and are observed within the solid angle of the observer. Secondly, the number

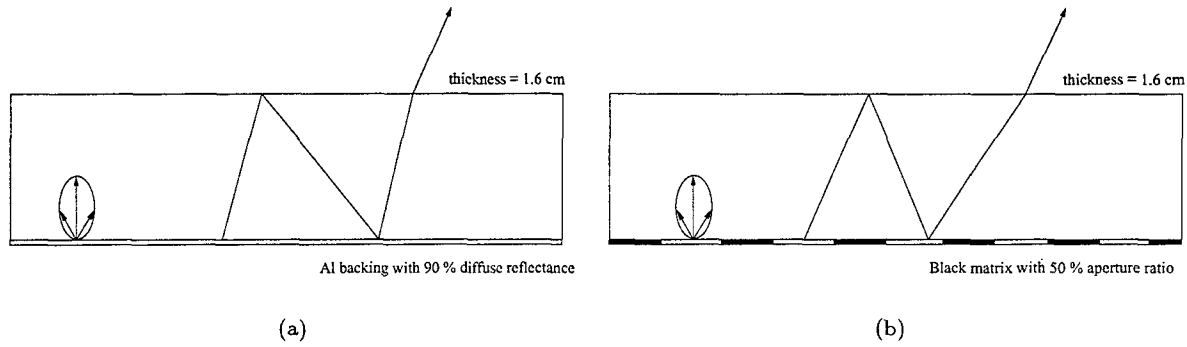


Figure 2: Cross-sections of emissive structures CRT-A (a) , and CRT-B (b).

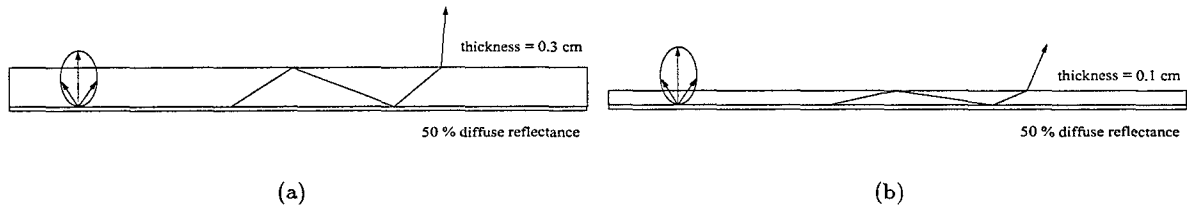


Figure 3: Cross-sections of emissive structures FPD-A (a), and FPD-B (b).

of photons observed within the solid angle of the observer but last associated with a point on the emission layer which is located at a radius from  $r$  to  $\Delta r$  from the source point are binned within  $N$  bins out to a distance  $N\Delta r$  ( $P_i$  for  $i = 1..N$ ). This is then converted to the differential probability of light emission per unit area,

$$L(i) = \frac{dL}{dA}$$

$$L(i) = \frac{P_i/P_0}{\pi[(i+1)\Delta r]^2 - (i\Delta r)^2]}$$

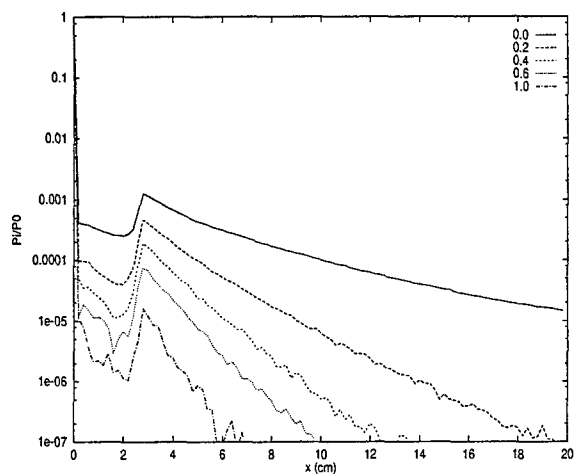
for,

$$r = i\Delta r$$

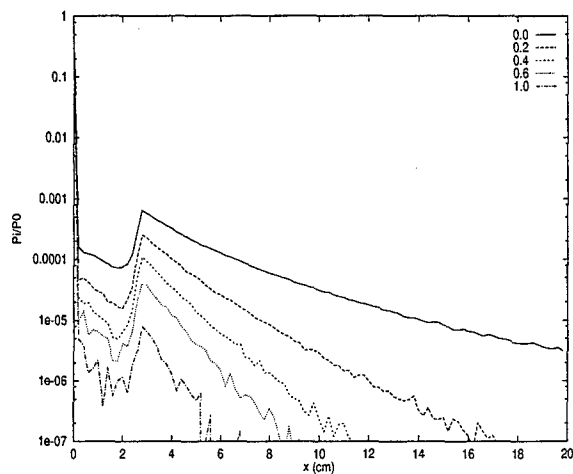
$$i = 1..N$$

where  $L(i)$  is a discrete representation of the continuous luminance point spread function  $L(r)$ .  $L(r)$  can be interpreted as the observed luminance in  $\text{cd}/\text{m}^2$  resulting from a point source located at the origin of the emissive surface with a luminous intensity of 1 cd.

Because  $L(0)$  is associated with a point source and goes to a very large number when small  $\Delta r$  are used for the binning of the Monte Carlo code, we define  $L(i)$  only for values of  $i$  ranging from 1 to  $N$ . Instead, the luminous intensity of the central peak,  $I(0)$ , was defined as the fraction of unscattered light that reaches the viewer from a point source producing a luminous intensity of 1 cd.  $I(0)$  describes the brightness of images not degraded by glare. For a digital display, the luminance associated with an emissive structure having an apparent luminous intensity of  $I(0)$  per pixel is  $I(0)/\rho_p$ , where  $\rho_p$  is the number of pixels per  $\text{m}^2$ .  $I(0)$  can be deduced from  $P_0$  and the lumens of light associated with the number of histories started at the phosphor layer. For the emissive structures studied in this work,  $P_0$  is the same in the absence of absorbers. We therefore have normalized  $I(0)$  to 1000. The relative reduction of  $I(0)$  with absorption is used as a measure of brightness.

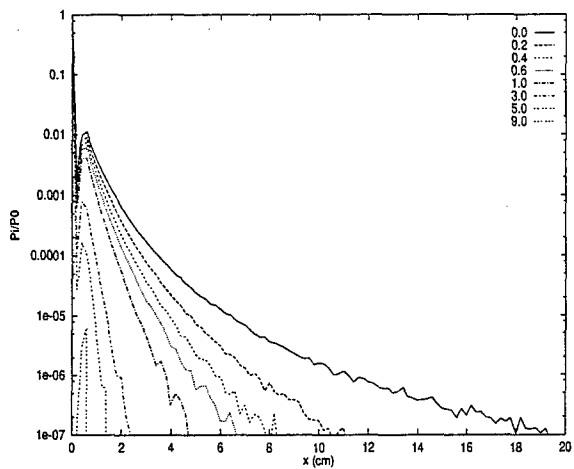


(a)

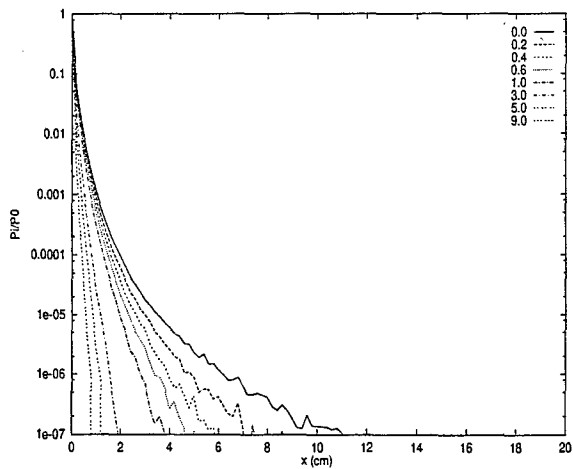


(b)

Figure 4:  $P_i/P_0$  for CRT-A (a), and CRT-B (b) computed for different absorption coefficients in  $\text{cm}^{-1}$  with  $\Delta r = 0.2$  cm.



(a)



(b)

Figure 5:  $P_i/P_0$  for FPD-A (a), and FPD-B (b) computed for different absorption coefficients in  $\text{cm}^{-1}$  with  $\Delta r = 0.2$  cm.

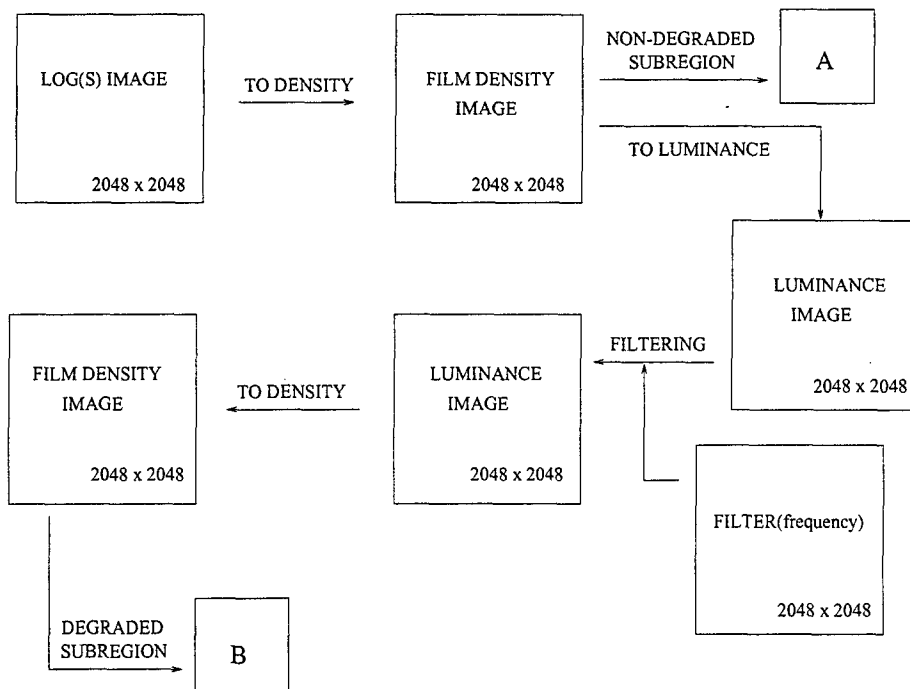


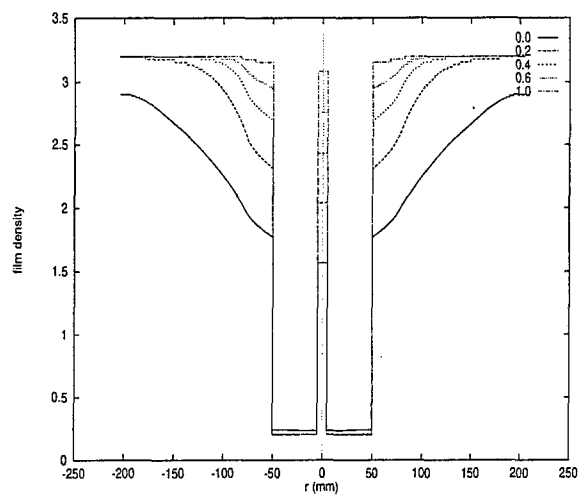
Figure 6: Processing steps for convolution of radiographic images with glare PSF.

Monte Carlo data was computed out to a distance of 20 cm for 100 bins with a spacing of 2 mm. A two dimensional point spread function ( $L(x, y)$ ) was interpolated from this for a 20 x 20 cm area with 2048 x 2048 pixels having dimensions of 0.2 x 0.2 mm. All points out to a radius of 2 mm were set equal to  $L(1)$ . The remaining points at larger radius were linearly interpolated from  $L(i)$ . All points other than the center point were then converted from  $\text{cd/m}^2$  to  $\text{cd/pixel}$  by multiplying each value by an area per pixel of  $0.04 \text{ mm}^2$  to correspond with digital images having a 0.2 mm pixel size. Finally, the point spread function was normalized so that the sum of all points in the 2-dimensional discrete array was 1.0. This insures that the convolution with the PSF preserves the average brightness of a displayed scene. Implicitly, the display of an image with high glare is thus assumed to be adjusted to preserve the same average brightness.

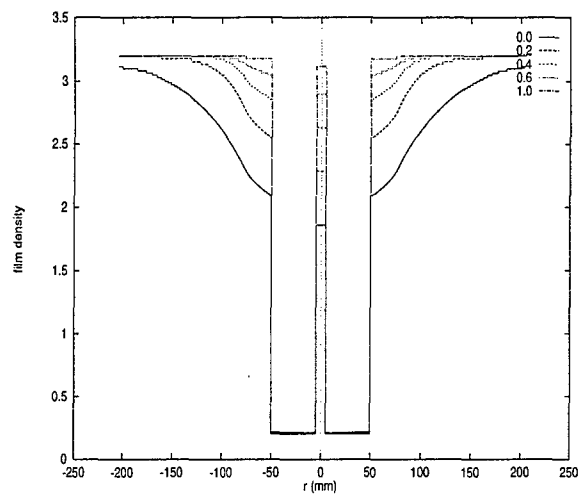
Figures 4 and 5 show the  $P_i/P_0$  of the 4 emissive structures computed in this work. The amplitude of the tails of these functions decreases with the absorption level. For CRT-A, the tail extends up to a distance of 20 cm, with a large amplitude for low absorption levels. For CRT-B, the overall same profile is observed, although the tail amplitudes are lower and decrease more rapidly with distance as compared to the PSFs of CRT-A. For the flat-panel emissive structures, tails have a greater amplitude close to the origin and a rapid fall-off. For the thinner structure (FPD-B), the amplitudes of the tails are still significant close to the origin but rapidly decay to very low numbers with distance.

### 3.2 Computational simulation of glare for displayed radiographs

In this study, we assumed that the display of radiographs in electronic devices can be modeled by convolving radiographic images in luminance units with the 2-dimensional PSF,  $L(x, y)$ . The convolution process is performed on images in luminance units, since the degrading effect of glare is linear after the visible light has been generated in the phosphor layer. For simulation purposes, images in film density units are first obtained by (a) computationally generating a test pattern image of film density, (b) digitizing available radiographic films, or (c) converting CR

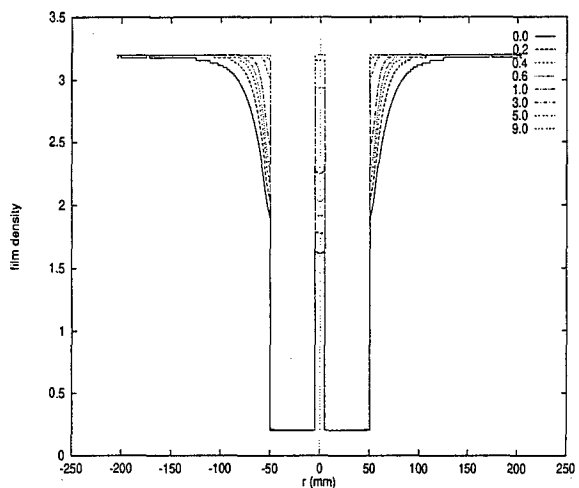


(a)

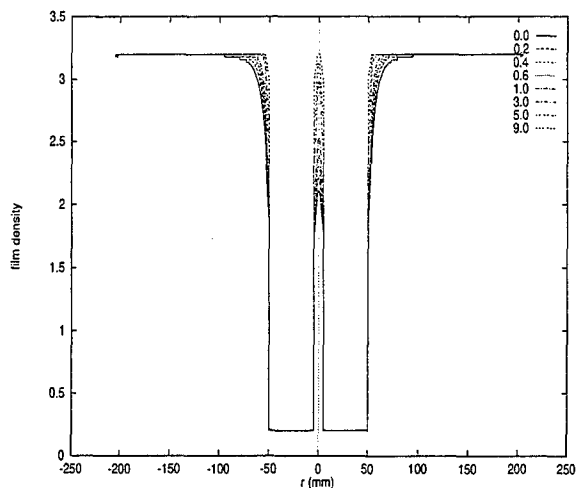


(b)

Figure 7: Test pattern image center data row for different absorption coefficients in  $\text{cm}^{-1}$  after convolution with PSFs of CRT-A (a), and CRT-B (b).



(a)



(b)

Figure 8: Test pattern image center data row for different absorption coefficients in  $\text{cm}^{-1}$  after convolution with PSFs of FPD-A (a), and FPD-B (b).



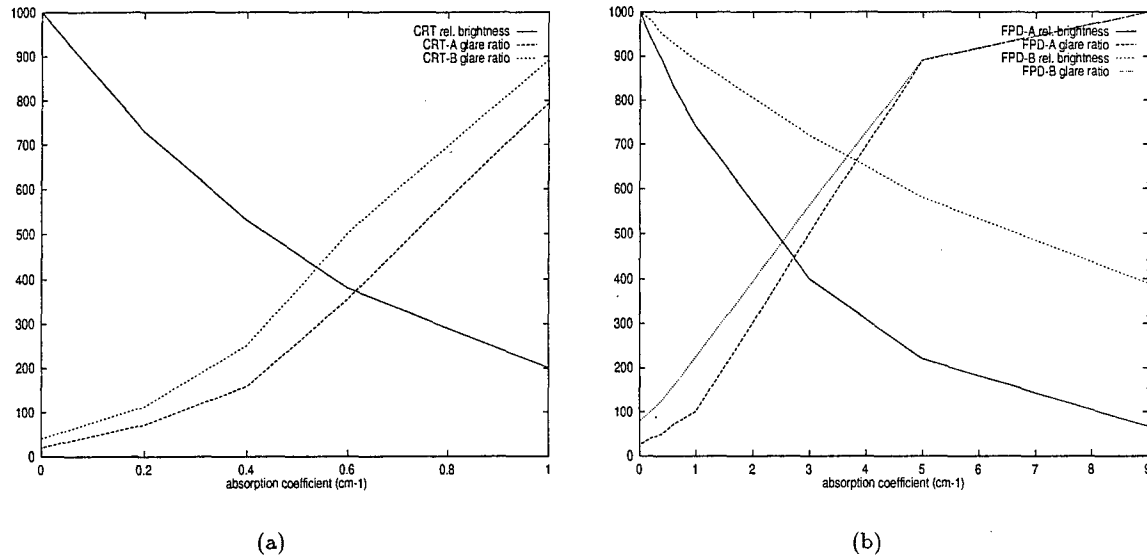


Figure 9: Glare ratios and central pixel relative brightness as a function of absorption coefficient for (a) CRT, and (b) flat-panel emissive structures.

data in units of  $\log(\text{signal})$  to film density units using parameterized HD curves. These images were then converted from density to luminance units using the following relationship:  $L = L_{max} * 10^{-FD}$ , where  $L_{max}$  is the viewbox luminance (assumed at 3000 cd/m<sup>2</sup>), and  $FD$  is the film density.

To simulate the degradation of image quality by glare, 2K x 2K images were convolved in the frequency domain with 2K x 2K filters generated from  $L(x, y)$ . Because  $L(x, y)$  has extended tails,  $L(x, y)$  arrays of 4K x 4K are needed for exact solutions. Our use of 2K x 2K kernels may introduce aliasing artifacts, although none were observed in the images studied to date.

$L(x, y)$  was first transformed using a 2-dimensional fast Fourier transform (FFT). Since this function is symmetric, we stored the magnitude of the Fourier coefficients in real arrays that were then used as filter functions. The 2K luminance images were read, Fourier transformed and filtered by multiplying the complex transformed image by the filter value. The complex array resulting from this multiplication was then converted back to luminance space by an inverse FFT procedure. After the convolution process was performed, images were converted back to film density units. All computations were performed on a DEC Alphastyle 2000. The convolution process for the 2K images including reading and writing operations, conversion to luminance units, FFT, filtering, inverse FFT and conversion to film density units was coded in fortran90 and required about 60 s per image. The processing steps are summarized in Fig. 6. Provision was made to extract a subregion in film density units from the undegraded and glare degraded image, i.e. A and B in Fig. 6. This was done to permit observer studies where A and B are printed on film using a laser printer.

Using this method, circular test patterns of the type shown in Fig. 1 were convolved with the filters computed for the 4 emissive structures. Figures 7 and 8 show the results of computed film density along a row through the center of a test pattern with a 10 cm diameter bright circle with a 1 cm diameter dark center. A diffuse glare component can be seen surrounding the bright circle with the amount of glare being inversely related to the amount of absorber. The glare ratio was computed as the ratio of the luminance in the bright area to the luminance in the dark spot. Figure 9 shows the reduction in glare and improvement in glare ratio that can be achieved by increasing the amount of absorbers. Also shown is the decrease in overall brightness caused by absorption.

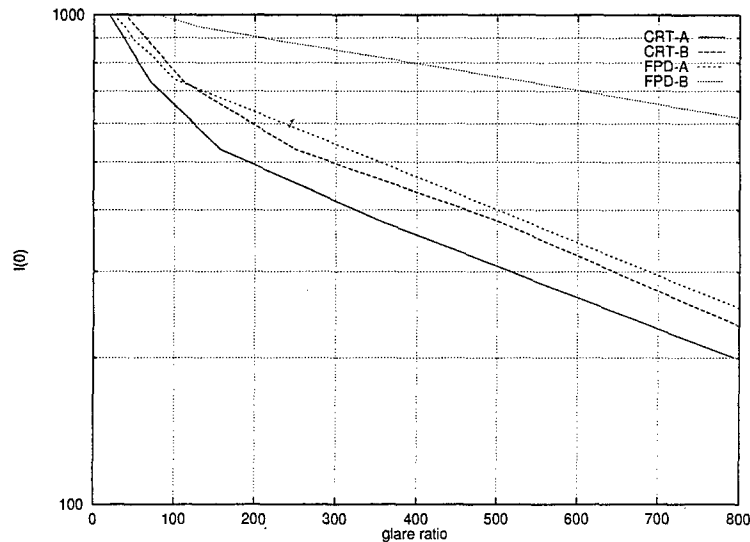


Figure 10: Relative brightness as a function of glare ratio for emissive structures CRT-A, CRT-B, FPD-A, and FPD-B.

## 4 DISCUSSION

In this study we computed results for circular test patterns of 4 cm diameter and 20 cm diameter in addition to the reported results for 10 cm diameter. The glare ratios measured for the different patterns are different because the component in the dark center is integrated over a larger radius. Further work should be done to identify which test pattern is best with respect to predicting adverse glare degradation in clinical radiographs.

We have conducted preliminary studies using clinical radiographs obtained from a digital radiography system. For both chest and skeletal radiographs, small lesions were added to the  $\log(\text{signal})$  data in regions where glare degradation was anticipated. Subjective observation of this data indicates that a glare ratio of 250 measured with a 10 cm diameter test pattern does not create appreciable degradation in the clinical image. Further work will be necessary to understand how differing amounts of glare impact radiologic observation.

From our results it is apparent that emissive structures which are designed to minimize glare will have reduced brightness. This is illustrated in Fig. 10 where we have plotted the relative brightness,  $I(0)$ , as a function of the glare ratio for all cases considered. For the same glare ratio, the black matrix structure is seen to perform better than a conventional monochrome CRT although in this simulation we have not accounted in differences of phosphor luminous efficiency. Notably, a significant improvement is seen in very thin flat panel displays for which the high frequency of multipath reflections allow the phosphor to damp the tail of the PSF.

## 5 ACKNOWLEDGMENTS

This work was partially supported by an U.S. Army Breast Cancer research grant.

## 6 REFERENCES

- [1] M. J. Flynn, T. McDonald, E. DiBello, E. Jorgensen, and W. Worobey. Flat panel display technology for high performance radiographic imaging. In *SPIE Medical Imaging 1995*, volume 2431-33, 1995.
- [2] D. Gur. Experience with CRT displays in the Radiology Department. *SID'91 Digest*, pages 353-354, 1991.
- [3] E. Muka and H. Blume. Display of medical images on CRT displays. In *SPIE Medical Imaging 1995*, 1995.
- [4] H. Roehrig, H. Blume, T. L. Ji, and M. Browne. Noise of CRT display systems. In *SPIE Medical Imaging 1993: Image Capture, Formatting and Display*, volume 1897, pages 232-245, 1993.
- [5] H. Blume, H. Roehrig, T. Lan Ji, and M. Browne. Very-high-resolution monochrome CRT displays. *SID'91 Digest*, pages 355-358, 1991.
- [6] H. Blume. Very-high-resolution CRT display systems. *SID'92 Digest*, pages 699-702, 1992.
- [7] A. Imamura, T. Ikoma, H. Makio, and K. Kikuchi. Very-high-resolution CRT display systems. *SID'92 Digest*, pages 501-504, 1992.
- [8] Clinton Electronics Corporation. *CRT design guide*.
- [9] C. Ajluni. FED technology takes display industry by storm. *Electronics design*, pages 56-66, October 1994.
- [10] K. Derbyshire. Beyond AMLCDs: field emission displays? *Solid State Technology*, pages 55-65, November 1994.
- [11] C. Ajluni. Can FED "Davids" vanquish the AMLCD "Goliaths"? *Thin-film Technology*, pages S3-S8, December 1996.
- [12] Francis Courreges. Parameters in FED product design. *Journal of the Society of Information Display*, pages 10-12, November 1996.
- [13] Henry F. Gray. The field-emitter display. *Journal of the Society of Information Display*, pages 9-14, March 1993.
- [14] E. Muka, T. Mertelmeier, R. Slone, and E. Senol. Impact of image noise and phosphor granularity on the specification of high-resolution medical image CRT displays. In *SPIE Medical Imaging 1997*, 1997.
- [15] T. Mertelmeier and T. E. Kocher. Monitor simulations for the optimization of medical soft-copies. In *SPIE Medical Imaging 1996: Image Display*, volume 2707, pages 322-333, 1996.
- [16] G. Spekowius, M. Weibrecht, C. D'adda, A. Antonini, C. Casale, and H. Blume. A new high brightness monochrome monitor based on color CRT technology. *SPIE: Medical Imaging 1997*, 1997.
- [17] A. Badano, M. J. Flynn, E. Samei, and K. G. Kearfott. Performance of low-voltage phosphors in emissive flat panel displays for radiologic applications. In *SPIE Medical Imaging 1996: Image Display*, volume 2707, pages 312-321, 1996.
- [18] P. Hovington, D. Drouin, and R. Gauvin. CASINO: A new Monte Carlo code in C language for electron beam interaction - Part I: Description of the program. *Scanning*, 19:1-14, 1997.
- [19] D. C. Joy. A database on electron-solid interactions. *Scanning*, 17:270-275, 1995.

# MONTE CARLO MODELING OF THE LUMINANCE SPREAD FUNCTION IN FLAT PANEL DISPLAYS

Aldo Badano and Michael J. Flynn

X-Ray Imaging Research Laboratory, Henry Ford Health System, Detroit, MI  
Dept. of Nuclear Engineering and Radiological Sciences, University of Michigan, Ann Arbor, MI

## ABSTRACT

The luminance spread function of thin emissive displays has been modeled using an optical Monte Carlo code to describe light transport. Line-spread and modulation transfer functions have been computed for different emissive structure thicknesses. Simulation of image degradation performed by a convolution process showed that even for very thin faceplates, control of lateral light diffusion is needed to minimize the contrast degradation by glare. When compared to thick emissive structures typical of cathode-ray tubes, thin structures are found to be capable of high quality due to more frequent absorption by the phosphor layer.

## I. INTRODUCTION

For some applications such as graphic arts and medical imaging, display devices with very good image quality are required. High brightness, low noise, wide luminance range and low glare are specifically required for digital radiographic display devices.<sup>5</sup> To depict good contrast over the wide range of signals in a digital radiograph requires a dynamic range of 100. To minimize the degradation of contrast in regions of minimum luminance, the glare from surrounding bright regions should be less than 0.25 of the minimum luminance (i.e., 1/400 of the maximum luminance). This work examines the design requirements for achieving this low glare in thin emissive display devices.

Currently, workstations designed for displaying and interpreting digital radiographs all use cathode ray tube devices (CRTs). Multipath light scattering in CRT faceplates causes extended tails in the luminance spread function.<sup>6,1</sup> Black matrix coatings and glass absorption are approaches that have been used to control glare from optical scattering at the expense of display brightness. In addition to the optical transport processes, electron backscattering in the vacuum tube has been reported to contribute to glare.<sup>4,10</sup> In general, the image quality of CRT devices has not been adequate for displaying digital radiographs in medical diagnostic applications.

On the other hand, flat emissive displays have the potential for better image quality than is possible with a CRT. For these devices a thin faceplate can be employed due to the large number of spacers between the

electron emitting layer and the phosphor. Extended electron backscattering is not present and lateral transport of optical photons can be controlled more effectively. For thin emissive structures, no results have been reported on the optical transfer characteristics and its effect on glare, brightness, and resolution. In this paper, we examine the optical transport processes in the faceplate of thin emissive display devices and its effect on low frequency image signals. The effect of glare for flat panel emissive structures is computationally modeled and the characteristics of the luminance spread functions are reported. In addition, the influence of glass absorption on glare and display brightness is analyzed.

The point spread function and modulation transfer function (MTF) are commonly used to describe the resolution of imaging devices. The glare in a display device may also be described by the point spread function if care is taken to document the low signals in the tail of the function which can extend for considerable distances. These tails are associated with a low frequency drop in the MTF which can be used to describe contrast reduction due to glare. We have used numeric Monte Carlo methods in this work to deduce the 2-dimensional (2D) point spread function of specific systems over distances equal to the full display size. This is then used to evaluate measures of image quality.

## II. COMPUTATIONAL METHODS

### A. Luminance spread function

The modeling of the light transport processes that occur in emissive structures can be done using either ray tracing or Monte Carlo methods. Ray tracing techniques rely upon a priori knowledge of the system response to determine the principal ray paths that will contribute to the output. On the other hand, Monte Carlo methods track the trajectories of a large number of optical photons to describe the statistically averaged output. Absorption and scattering processes are modeled with the Monte Carlo method by randomly sampling the distance to each event from probability distribution functions. Absorption and scattering are described by linear interaction coefficients ( $\text{cm}^{-1}$ ). Monte Carlo methods can handle a wide variety of physical cases and are computationally practical when using high speed computers.

To model the luminance spread functions in emissive displays, we have developed a Monte Carlo optical transport code written in fortran 90 (Detect-II). The geometry is described in 3D cartesian coordinates using slabs with orthogonal division into volumetric cells. The surface definitions include rough surfaces, mirrors, perfect absorbers, partial diffuse absorbers with lambertian emission and thin films. Photon histories are started as point or planar sources with lambertian or isotropic angular distribution. Individual photons are allowed to be absorbed or scattered in the medium. A unique feature of Detect-II is the tracking of photon polarization. In very thin structures, multiple light reflections occur, and polarization dependencies in the Fresnel coefficients have to be considered.

Neglecting the effect of finite wavelength, the light transport is simulated by tracking individual photons using a physical optics description. Reflection and transmission coefficients given by Fresnel's equations are then interpreted as probabilities. The transmission and reflection probabilities for parallel and perpendicular components are:<sup>3</sup>

$$P_{\parallel,T} = \frac{\sin(2\theta_1)\sin(2\theta_2)}{\sin^2(\theta_1 + \theta_2)\cos^2(\theta_1 - \theta_2)}$$

$$P_{\perp,T} = \frac{\sin(2\theta_1)\sin(2\theta_2)}{\sin^2(\theta_1 + \theta_2)}$$

$$P_{\parallel,R} = \frac{\tan^2(\theta_1 - \theta_2)}{\tan^2(\theta_1 + \theta_2)}$$

$$P_{\perp,R} = \frac{\sin^2(\theta_1 - \theta_2)}{\sin^2(\theta_1 + \theta_2)}$$

where  $\theta_1$  is the incidence angle and  $\theta_2$  is given by Snell's law.

An important aspect of the code is a method for binning results which is designed for display modeling. To simulate display performance, the viewer is assumed to observe the image from a direction normal to the surface. Photons are tracked from the source to the front surface of the display and those within a finite solid angle about the normal are binned into discrete regions on the surface. A solid angle corresponding to a  $6^\circ$  cone is used rather than the typical solid angle of a human observer in order to make efficient use of the photon histories. The binning of the emerging position is done by backprojecting the light path to a virtual plane of emission. This accounts for the difference in index of refractions between air and glass. This allows binning from a large solid angle to a common virtual focal plane inside the emissive structure.

To avoid correlations in multidimensional space when a large number of histories are needed, a portable, very-long period ( $2^{144}$ ) lagged Fibonacci random number generator is used.<sup>8,7</sup>

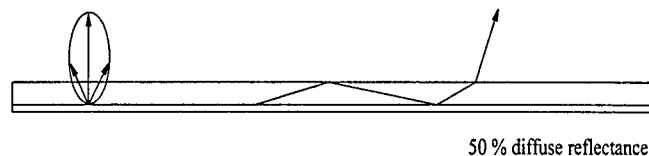


Fig. 1. Cross-section of thin emissive structure model.

In a thin cathodoluminescent display device, the emissive structure includes all components that convert energetic electrons to visible light. Typical emissive structures components include: cathodoluminescent phosphors, conductive layers, reflective or absorptive films, transparent support (faceplate), and antireflective and antiglare coatings. In this work, we have modeled the glare characteristics of thin emissive structures with different faceplate thicknesses (0.5, 1.0, 2.0, and 3.0 mm) and for absorption levels (0.0, 1.0, 3.0, 5.0, 9.0, and  $12.0 \text{ cm}^{-1}$ ). All surfaces are modeled as perfectly flat. Light entering the phosphor layer is assumed to return into the faceplate with a probability of 0.5 with a lambertian angular distribution. A cross-section of the emissive structure is presented in figure 1.

In previous work, we described methods to obtain the 2D luminance spread function from the Monte Carlo results.<sup>1</sup> A brief summary is given in this paragraph to facilitate the interpretation of the results presented in this paper. The Monte Carlo calculation yields the number of photons,  $P_0$ , that originate from the source point and are observed within the solid angle of the observer associated with a point on the emission layer which is located at a radius from  $r$  to  $\Delta r$  from the source point. This is then converted to the discrete differential probability of light emission per unit area  $L(i)$ , which is a discrete representation of the continuous luminance spread function  $L(r)$ .  $L(r)$  can be interpreted as the observed luminance in  $\text{cd}/\text{m}^2$  resulting from a point source located at the origin of the emissive surface with a luminous intensity of 1 cd. For the central peak,  $I(0)$ , is defined as the fraction of unscattered light that reaches the viewer from a point source producing a luminous intensity of 1 cd.  $I(0)$  describes the brightness of images not degraded by glare.

### B. Image processing

We use the 2D luminance spread function to simulate image degradation by convolving this function with values for an image scene. These convolutions are done in the frequency domain using a 2D Fourier transform. To

describe the degradation both the line-spread function (LSF) and the MTF are deduced. The 1D luminance LSF is computed by projecting the 2D luminance spread function and normalizing the 1D vector to unity. A 1D Fourier transform is then performed on the LSF to obtain the MTF.

Glare measurements on CRT emissive structures are commonly performed with a large bright region and a small black spot.<sup>9,4,10</sup> The ratio of luminances in the bright field and the dark spot is defined as the glare ratio. The results of these glare measurements are strongly dependent on the nature of the test image. However, no standard metric has been adopted for reporting the glare characteristics of actual display devices. In this study, we use a circular test pattern that we have previously described.<sup>2</sup> The pattern consists of an inner dark circular spot, surrounded by a bright outer circle with a ratio of radii of 10. The rest of the scene is kept at the same dark level of the inner spot. The glare ratio is defined as the difference in display luminance between the central pixel in the pattern and the brightest pixel in the bright region.

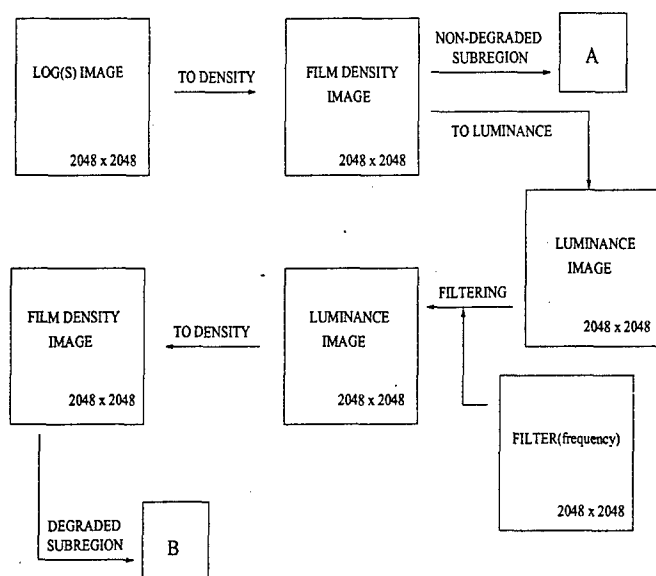


Fig. 2. Processing steps for simulation of image quality degradation by glare by convolution with luminance spread functions

A high fidelity display device should replicate the appearance of transilluminated film. To model this, we assume that the display of radiographs in an electronic device can be modeled by convolving radiographic images in luminance units with an interpolated 2D PSF. Glare pattern images are first converted from film density to luminance units using the following relationship:

$$L = L_{max} * 10^{-FD}$$

where  $L_{max}$  is the viewbox luminance (assumed at 3000 cd/m<sup>2</sup>), and  $FD$  is the film density. The convolution process is then performed on images in luminance units, since the degrading effect of glare is linear after the visible light has been generated in the phosphor layer (see figure 2). To simulate the degradation of image quality by glare,  $2K \times 2K$  images were convolved in the frequency domain with  $2K \times 2K$  filters generated from the 2D PSF.<sup>1</sup>

### III. RESULTS AND DISCUSSION

Figure 3 shows the LSF of emissive structures considered in this work with no glass absorption. For thin emissive structures with faceplate thickness less than 3 mm, the LSFs show high amplitudes close to the origin with tails that decay rapidly to very low numbers. Moreover, the LSF for 0.5 and 1 mm have similar features, differing only at large distances and very close to the origin. At 3 mm, a peak is observed that defines a halo around the center spot. The amplitudes at short distances are lower than for thinner faceplates by a factor of at least 0.25. In figure 4, the MTFs of the same emissive structures are plotted. The drop in amplitude is approximate constant for all frequencies, up to the Nyquist limit.

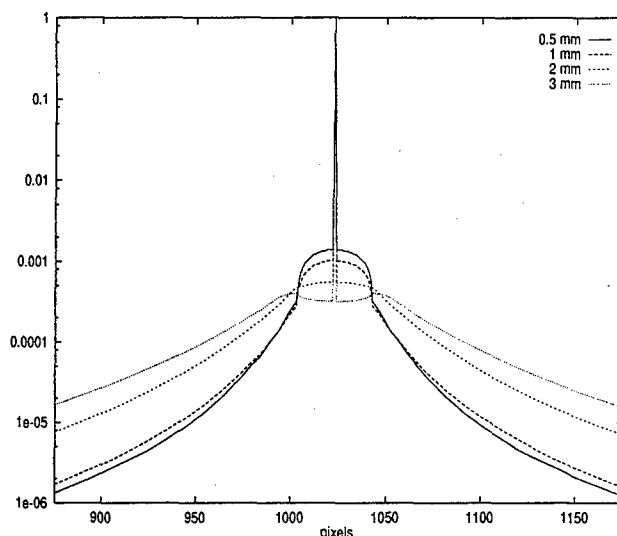


Fig. 3. Line-spread functions for different faceplate thicknesses with no glass absorption (for a pixel size of 0.2 mm).

To determine if an emissive structure is capable of achieving the high glare ratio needed for radiologic interpretation (i.e., about 400), we have computed test pattern glare ratios for emissive structures of different thicknesses and with different absorption levels.

Figure 5 illustrates the relative brightness  $I(0)$  as a function of the glare ratio for the emissive structures

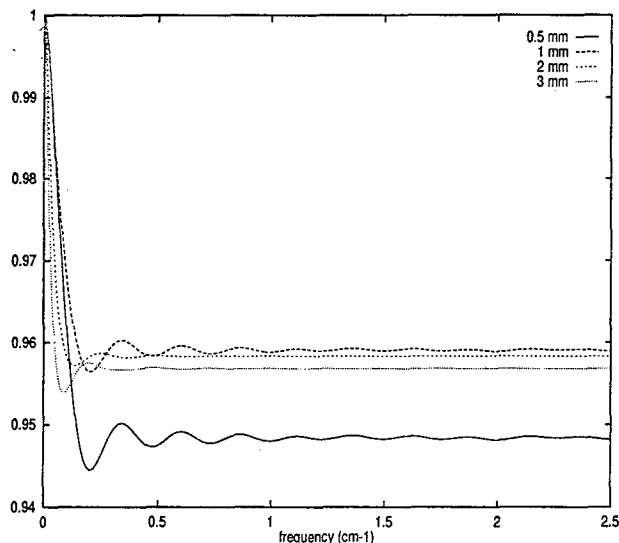


Fig. 4. Modulation transfer functions for different faceplate thicknesses with no glass absorption (for a pixel size of 0.2 mm).

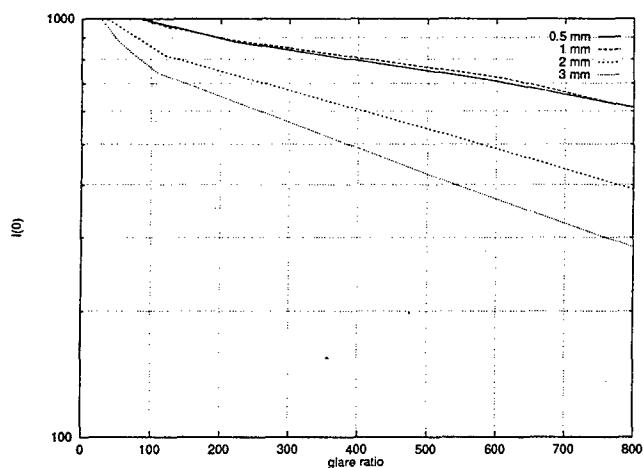


Fig. 5. Relative brightness as a function of the glare ratio for different faceplate thicknesses. For each curve, glass absorption is varied to decrease  $I(0)$  and increase the glare ratio.

considered. Higher glare ratios are possible to achieve by increasing the absorption level, although decreasing brightness. To obtain a given glare ratio, an increase in faceplate thickness results in a reduction of the display brightness. For a glare ratio of 400, the brightness has to be reduced by 37.5 % if the thickness of the emissive structure is increased from 1 to 3 mm. Again, similar characteristics are observed for faceplate thicknesses of 0.5 and 1 mm. As seen in figure 3, the similar features in the LSFs may be responsible for the similarities in the achievable brightness for a given glare ratio.

#### IV. SUMMARY

The luminance spread functions of thin emissive structures typical of flat cathodoluminescent displays have been modeled with an optical Monte Carlo code. The tails of the spread functions show that even for thin structures, the light scattering within these structures has to be controlled in order to achieve glare ratios suitable for high performance applications. The use of absorption in the faceplate has been shown to be a possible solution, although affecting the display brightness. Other solutions may include the use of a black matrix coating in between the phosphor dots.

#### V. ACKNOWLEDGEMENTS

This work was partially supported by a U.S. Army Breast Cancer research grant.

#### REFERENCES

- [1] A. Badano and M. J. Flynn. Image degradation by glare in radiologic display devices. In *SPIE Medical Imaging 1997: Image Display*, 1997.
- [2] A. Badano, M. J. Flynn, E. Samei, and K. J. Kearfott. Performance of low-voltage phosphors in emissive flat panel displays for radiologic applications. In *SPIE Medical Imaging 1996: Image Display*, volume 2707, pages 312-321, 1996.
- [3] M. Born and E. Wolf. *Principles of optics*. 3rd. revised edition, 1965.
- [4] G. C. de Vries. Contrast-enhancement under low ambient illumination. *SID'95 Digest*, pages 32-35, 1995.
- [5] M. J. Flynn, T. McDonald, E. DiBello, E. Jorgensen, and W. Worobey. Flat panel display technology for high performance radiographic imaging. In *SPIE Medical Imaging 1995*, volume 2431-33, 1995.
- [6] E. B. Gindele and S. L. Shaffer. A physical optics CRT faceplate halation model. *SID'91 Digest*, pages 446-450, 1991.
- [7] F. James. A review of pseudorandom number generators. *Computer Physics Communications*, 60:329-344, 1990.
- [8] G. Marsaglia, A. Zaman, and W.W. Tsang. Toward a universal random number generator. *Statistics and Probability Letters*, 8:35-39, 1990.
- [9] G. Spekowius, M. Weibrecht, C. D'adda, A. Antonini, C. Casale, and H. Blume. A new high brightness monochrome monitor based on color CRT technology. *SPIE: Medical Imaging 1997*, 1997.
- [10] J. J. van Oekel. Improving the contrast of CRTs under low ambient illumination with a graphite coating. *SID'95 Digest*, pages 427-430, 1995.



DEPARTMENT OF THE ARMY  
US ARMY MEDICAL RESEARCH AND MATERIEL COMMAND  
504 SCOTT STREET  
FORT DETRICK, MARYLAND 21702-5012

REPLY TO  
ATTENTION OF:

MCMR-RMI-S (70-1y)

23 Aug 01

MEMORANDUM FOR Administrator, Defense Technical Information  
Center (DTIC-OCA), 8725 John J. Kingman Road, Fort Belvoir,  
VA 22060-6218


SUBJECT: Request Change in Distribution Statement

1. The U.S. Army Medical Research and Materiel Command has reexamined the need for the limitation assigned to the technical reports listed at enclosure. Request the limited distribution statement for these reports be changed to "Approved for public release; distribution unlimited." These reports should be released to the National Technical Information Service.

2. Point of contact for this request is Ms. Judy Pawlus at DSN 343-7322 or by e-mail at judy.pawlus@det.amedd.army.mil.

FOR THE COMMANDER:

Encl

  
PHYLLIS M. RINEHART  
Deputy Chief of Staff for  
Information Management



Reports to be Downgraded to Unlimited Distribution

ADB241550	ADB253628	ADB249654	ADB263448
ADB251657	ADB257757	ADB264967	ADB245021
ADB263525	ADB264736	ADB247697	ADB264544
ADB222448	ADB255427	ADB263453	ADB254454
ADB234468	ADB264757	ADB243646	
ADB249596	ADB232924	ADB263428	
ADB263270	ADB232927	ADB240500	
ADB231841	ADB245382	ADB253090	
ADB239007	ADB258158	ADB265236	
ADB263737	ADB264506	ADB264610	
ADB239263	ADB243027	ADB251613	
ADB251995	ADB233334	ADB237451	
ADB233106	ADB242926	ADB249671	
ADB262619	ADB262637	ADB262475	
ADB233111	ADB251649	ADB264579	
ADB240497	ADB264549	ADB244768	
ADB257618	ADB248354	ADB258553	
ADB240496	ADB258768	ADB244278	
ADB233747	ADB247842	ADB257305	
ADB240160	ADB264611	ADB245442	
ADB258646	ADB244931	ADB256780	
ADB264626	ADB263444	ADB264797	